A&A 619, L3 (2018)
https://doi.org/10.1051/0004-6361/201834091

Astronomy & Astrophysics

LETTER TO THE EDITOR

(16) Psyche: A mesosiderite-like asteroid?⋆,⋆⋆

M. Viikinkoski[1], P. Vernazza[2], J. Hanuš[3], H. Le Coroller[2], K. Tazhenova[2], B. Carry[4], M. Marsset[5], A. Drouard[2], F. Marchis[6], R. Fetick[2], T. Fusco[2], J. Ďurech[3], M. Birlan[7], J. Berthier[7], P. Bartczak[8], C. Dumas[9], J. Castillo-Rogez[10], F. Cipriani[11], F. Colas[7], M. Ferrais[13], J. Grice[4,14], E. Jehin[13], L. Jorda[2], M. Kaasalainen[1], A. Kryszczynska[8], P. Lamy[12], A. Marciniak[8], T. Michalowski[8], P. Michel[4], M. Pajuelo[7,15], E. Podlewska-Gaca[8,16], T. Santana-Ros[8], P. Tanga[4], F. Vachier[7], A. Vigan[2], B. Warner[17], O. Witasse[11], and B. Yang[18]

[1] Laboratory of Mathematics, Tampere University of Technology, PO Box 553, 33101 Tampere, Finland
e-mail: matti.viikinkoski@tut.fi
[2] Aix Marseille Univ, CNRS, LAM, Laboratoire d'Astrophysique de Marseille, Marseille, France
[3] Astronomical Institute, Faculty of Mathematics and Physics, Charles University, V Holešovičkách 2, 18000 Prague, Czech Republic
[4] Université Côte d'Azur, Observatoire de la Côte d'Azur, CNRS, Laboratoire Lagrange, France
[5] Astrophysics Research Centre, Queen's University Belfast, BT7 1NN, UK
[6] SETI Institute, Carl Sagan Center, 189 Bernado Avenue, Mountain View, CA 94043, USA
[7] IMCCE, Observatoire de Paris, PSL Research University, CNRS, Sorbonne Universités, UPMC Univ Paris 06, Univ., Lille, France
[8] Astronomical Observatory Institute, Faculty of Physics, A. Mickiewicz University, Sloneczna 36, 60-286 Poznan, Poland
[9] Thirty-Meter-Telescope, 100 West Walnut St, Suite 300, Pasadena, CA 91124, USA
[10] Jet Propulsion Laboratory, California Institute of Technology, 4800 Oak Grove Drive, Pasadena, CA 91109, USA
[11] European Space Agency, ESTEC – Scientific Support Office, Keplerlaan 1, Noordwijk 2200 AG, The Netherlands
[12] Laboratoire Atmosphères, Milieux et Observations Spatiales, CNRS & Université de Versailles Saint-Quentin-en-Yvelines, Guyancourt, France
[13] Space sciences, Technologies and Astrophysics Research Institute, Université de Liège, Allée du 6 Août 17, 4000 Liège, Belgium
[14] Open University, School of Physical Sciences, The Open University, MK7 6AA, UK
[15] Sección Física, Departamento de Ciencias, Pontificia Universidad Católica del Perú, Apartado 1761, Lima, Perú
[16] Institute of Physics, University of Szczecin, Wielkopolska 15, 70-453 Szczecin, Poland
[17] Center for Solar System Studies, 446 Sycamore Ave., Eaton, CO 80615, USA
[18] European Southern Observatory (ESO), Alonso de Cordova 3107, 1900 Casilla Vitacura, Santiago, Chile

Received 15 August 2018 / Accepted 24 September 2018

ABSTRACT

Context. Asteroid (16) Psyche is the target of the NASA Psyche mission. It is considered one of the few main-belt bodies that could be an exposed proto-planetary metallic core and that would thus be related to iron meteorites. Such an association is however challenged by both its near- and mid-infrared spectral properties and the reported estimates of its density.
Aims. Here, we aim to refine the density of (16) Psyche to set further constraints on its bulk composition and determine its potential meteoritic analog.
Methods. We observed (16) Psyche with ESO VLT/SPHERE/ZIMPOL as part of our large program (ID 199.C-0074). We used the high angular resolution of these observations to refine Psyche's three-dimensional (3D) shape model and subsequently its density when combined with the most recent mass estimates. In addition, we searched for potential companions around the asteroid.
Results. We derived a bulk density of $3.99 \pm 0.26\,\mathrm{g\,cm^{-3}}$ for Psyche. While such density is incompatible at the 3-sigma level with any iron meteorites ($\sim 7.8\,\mathrm{g\,cm^{-3}}$), it appears fully consistent with that of stony-iron meteorites such as mesosiderites (density $\sim 4.25\,\mathrm{g\,cm^{-3}}$). In addition, we found no satellite in our images and set an upper limit on the diameter of any non-detected satellite of 1460 ± 200 m at 150 km from Psyche ($0.2\% \times R_{\mathrm{Hill}}$, the Hill radius) and 800 ± 200 m at 2000 km ($3\% \times R_{\mathrm{Hill}}$).
Conclusions. Considering that the visible and near-infrared spectral properties of mesosiderites are similar to those of Psyche, there is merit to a long-published initial hypothesis that Psyche could be a plausible candidate parent body for mesosiderites.

Key words. minor planets, asteroids: general – minor planets, asteroids: individual: (16) Psyche – methods: observational – techniques: high angular resolution

⋆ Based on observations made with 1) ESO Telescopes at the La Silla Paranal Observatory under programs 086.C-0785 (PI Carry) and 199.C-0074 (PI Vernazza); and 2) the *W. M. Keck* Observatory, which is operated as a scientific partnership among the California Institute of Technology, the University of California and the National Aeronautics and Space Administration. The Observatory was made possible by the generous financial support of the W. M. *Keck* Foundation.

⋆⋆ Tables A1 and A2 and reduced images are only available at the CDS via anonymous ftp to cdsarc.u-strasbg.fr (130.79.128.5) or via http://cdsarc.u-strasbg.fr/viz-bin/qcat?J/A+A/619/L3

1. Introduction

Asteroid (16) Psyche, the target of the NASA Discovery mission Psyche (Elkins-Tanton et al. 2017), is one of the very few main-belt asteroids that exhibits a relatively high radar albedo (0.42 ± 0.1, Shepard et al. 2010, 2015) and shallow phase-polarization minimum (Dollfus & Geake 1977; Dollfus et al. 1979), which imply that its surface/subsurface is metal-rich. On such a basis, it has been defined as a metallic world (Elkins-Tanton et al. 2017) and is considered one of the few main-belt bodies that could be an exposed planetary metallic core and that could thus be related to iron meteorites. This association is however challenged by both its near- and mid-infrared spectral properties and its density.

Spectroscopic observations in the near-infrared range have revealed the presence of (i) a weak (~1%) 0.9 μm absorption band suggesting the presence of orthopyroxene on its surface (e.g., Hardersen et al. 2005; Ockert-Bell et al. 2008; Sanchez et al. 2017) and (ii) a 3 μm absorption feature suggesting the presence of hydrated silicates on its surface (Takir et al. 2017). Spectroscopic observations with the *Spitzer* Space Telescope in the thermal infrared have provided additional evidence for the presence of fine-grained silicates at the surface of Psyche but have also detected the presence of a metallic bedrock (Landsman et al. 2018) consistent with earlier radar observations (Shepard et al. 2010). Finally, its thermal inertia is among the highest for an asteroid of this size (Matter et al. 2013). At this stage, one cannot exclude that some of the silicates (especially the hydrated ones) on the surface of the asteroid could have an exogenous origin (Avdellidou et al. 2018). We note that the presence of exogenous dust has already been reported at the surfaces of a number of large main-belt asteroids, including Vesta (Reddy et al. 2012) and Ceres (Vernazza et al. 2017).

What is more puzzling at this stage is the reported density for Psyche. Recent estimates of its density all fall in the 3.7–4.7 g cm^{-3} range (Hanus et al. 2017; Shepard et al. 2017; Drummond et al. 2018). Considering that large main-belt asteroids with a diameter greater than 200 km tend to have minimal macroporosity (≤10%, Carry 2012; Scheeres et al. 2015), one may expect this to be the case for Psyche ($D \sim 225$ km), which would significantly complicate a direct association between this asteroid and iron meteorites.

In the present study, we present high-angular-resolution imaging observations of Psyche with ESO VLT/SPHERE/ZIMPOL that were performed as part of our large program (ID 199.C-0074; PI: P. Vernazza). We use these observations to (i) refine Psyche's 3D shape model, and subsequently its density when combined with the most recent mass estimates, (ii) place for the first time constraints on the surface topography of the northern hemisphere of Psyche, and (iii) search for potential companions. Finally, we discuss what could be the most likely meteorite analog to Psyche.

2. Observations and data processing

We observed Psyche with VLT/SPHERE/ZIMPOL (Beuzit et al. 2008; Thalmann et al. 2008) at five different epochs, close to its opposition. Observational circumstances are listed in Table A.1. The data reduction was performed as described in Vernazza et al. (2018). Finally, the optimal angular resolution of each image was restored with the `Mistral` algorithm (Fusco et al. 2003; Mugnier et al. 2004).

Instead of using a stellar point-spread function (PSF) for the deconvolution, we used for the first time a parametric PSF with a Moffat shape (Moffat 1969). During our large program, deconvolution with the stellar PSF acquired just after the asteroid observation has sometimes led to unsatisfactory results. On some occasions, using stellar PSFs acquired on different nights improved the results.

We therefore tested deconvolution with PSFs modeled by a 2D Moffat function. Whereas the results of this Moffat-PSF deconvolution were similar to those obtained with the stellar PSF, the deconvolution with a Moffat PSF always converged toward satisfactory results (Fetick et al., in prep.). We therefore started systematically using a parametric PSF with a Moffat shape to deconvolve our images. The deconvolved images of asteroid Psyche are shown in Figs. 1 and A.1.

Lastly, for each epoch we produced an average image to increase the signal-to-noise ratio (S/N) and to perform a search for satellites (as we did for (41) Daphne, the first binary asteroid studied in our large program; see Carry et al. 2018).

3. Moon search around Psyche

We did not discover any companion around Psyche. As a subsequent step, we estimated the minimum diameter above which a moon would have been detected. Defining a threshold S/N at which the detection occurs is complex because 1) the diffracted light (generating background photon noise) is not symmetric around Psyche, 2) the instrumental speckle noise does not follow a normal law, and 3) the sample size is small (small number of pixels (Moffats-PSF) at any small separation with Psyche), thus preventing a robust statistical analysis.

To place an upper limit on the diameter of a companion, we simulated ten companions on a circle about on Airy disk away from the edge of the asteroid, where the photon noise from the diffracted light reaches its maximum value. The artificial moons were represented by normalized Airy disks multiplied by a constant flux to reach a local S/N of 1–3, and by the typical Strehl ratio of our observations of 0.7. The flux of each moon ($F_{\rm m}$) was then adjusted to be at the detection limit in each of our images. As such, a moon detectable around Psyche should have the following minimum diameter ($D_{\rm m}$):

$$D_{\rm m} > D_{16} \times \left(\frac{F_{\rm m}}{F_{16}}\right)^{(1/2)}, \quad (1)$$

where F_{16} is the integrated flux of Psyche and D_{16} is the surface-equivalent diameter of Psyche on the plane of the sky (that is 170 km). We found that any moon with a diameter $D_{\rm m}$ above 1460 ± 200 m at 150 km from the primary (or $0.2\% \times R_{\rm Hill}$, the Hill radius) would have been detected.

We also explored more remote orbits typical of large main-belt asteroids (at several primary radii; see Margot et al. 2015). At 100 pixels (about 2000 km) from Psyche, corresponding to $3\% \times R_{\rm Hill}$ where most of the satellites of 100+km asteroids have been found (Margot et al. 2015; Yang et al. 2016), the images are less affected by the diffracted light and we found that there should be no moon larger than $D_{\rm m} = 800 \pm 200$ m at these distances.

4. Size, shape and density

Recently, Shepard et al. (2017) derived a shape model of Psyche using range-Doppler imaging. The S/N of radar echoes was sufficient for identifying two crater-like depressions in the southern hemisphere, but the northern hemisphere remained unobserved

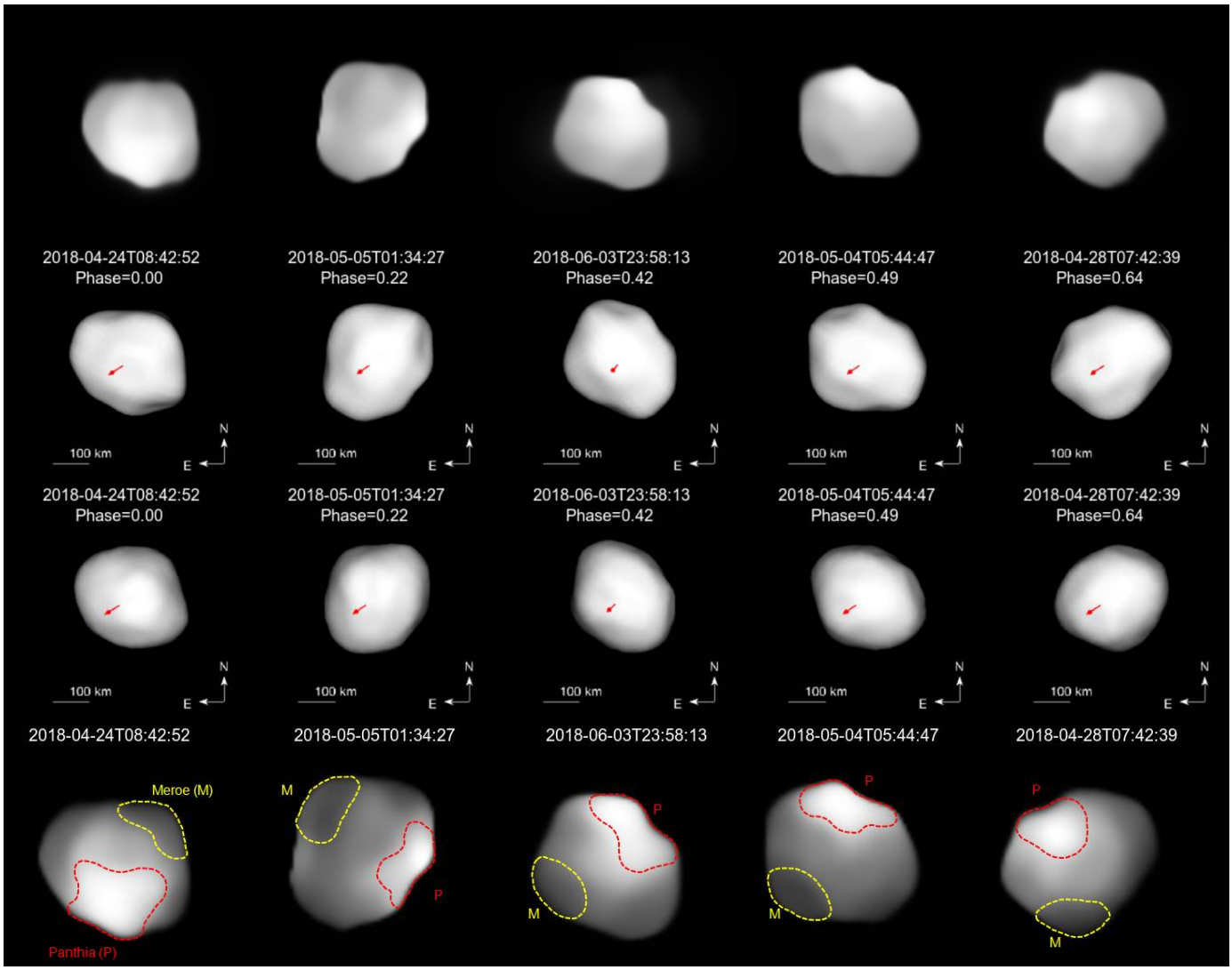

Fig. 1. *First row*: VLT/SPHERE/ZIMPOL images of Psyche obtained at five different epochs (ordered by rotation phase) and deconvolved with the `Mistral` algorithm and a parametric PSF with a Moffat shape (Sect. 2). *Second row*: corresponding shape model projections. *Third row*: corresponding projections using the shape model of Shepard et al. (2017). The arrow shows the direction of the rotation axis. *Last row*: images with contrast and size enhanced to highlight the albedo variegation. The two topographic regions that we consider as real features are also indicated.

and modeled with an ellipsoidal shape. Our SPHERE observations are highly complementary because they covered the northern hemisphere.

We used our All-Data Asteroid Modeling (`ADAM`) inversion technique (Viikinkoski & Kaasalainen 2014; Viikinkoski et al. 2015; Viikinkoski 2016; Hanus et al. 2017) to reconstruct the 3D shape model and the spin of Psyche. We utilized all available optical lightcurves (206), stellar occultations (2), and disk-resolved images (38). Our 25 VLT/SPHERE/ZIMPOL images were complemented by 11 *Keck*/NIRC2 and 2 VLT/NACO imaging epochs (Hanus et al. 2017; Shepard et al. 2017; Drummond et al. 2018), out of which 8 were taken under different sub-observer latitudes, complementary to our SPHERE images (Table A.1).

We also included two multiple-chord stellar occultations (Fig. A.2) recorded in 2010 and 2014 (Dunham et al. 2017). The 2014 occultation proved to be essential to constrain the size of the model along its rotation axis. Finally, we used a dataset of disk-integrated optical data consisting of 209 lightcurves in total: 118 lightcurves from van Houten-Groeneveld & van Houten (1958), Chang & Chang (1963), Tedesco & Taylor (1985), Taylor (1977), Tedesco et al. (1983), Lupishko et al. (1980, 1982), Zhou & Yang (1981), Zhou et al. (1982), Weidenschilling et al. (1987), Harris et al. (1999), Pfleiderer et al. (1987), Dotto et al. (1992), Weidenschilling et al. (1990), and Neely (1992), already used by Hanus et al. (2017), 3 lightcurves obtained by Warner (2016) in 2015, 85 lightcurves extracted from the SuperWASP image archive (Grice et al. 2017), and finally 3 lightcurves obtained in 2018 by Emmanuel Jehin in the Rc filter using the TRAPPIST South telescope.

The shape reconstruction was made more complex by discernible albedo variegation apparent both in the images and in the lightcurves. To model this phenomenon, we allowed each facet to have different relative brightness scaling parameters (i.e., to represent albedo variegation). Here, the albedo variegation was optimized simultaneously with the shape using both the lightcurves and imaging data, contrarily to Shepard et al. (2017) who used 114 lightcurves to fit albedo variegation to the fixed shape model. To avoid spurious spotty appearances, we defined a smoothing operator as a regularization term to discourage large deviations between neighboring facets. We chose, rather

Table 1. Physical parameters of Psyche derived in this study compared with previous works.

Parameter	K02/D11	S17	H17	D18	This work
D (km)	211 ± 21	226 ± 23	225 ± 4	223 ± 2	226 ± 5
λ (°)	32 ± 5	34 ± 5	28 ± 4	32 ± 3	34 ± 3
β (°)	-7 ± 5	-7 ± 5	-6 ± 3	-8 ± 3	-9 ± 3
P	4.195948(1)	4.195948(1)	4.195948(1)	4.195951(2)	4.195948(1)
a (km)		279 ± 27	293 ± 5	274 ± 2	290 ± 5
b (km)		232 ± 23	234 ± 5	231 ± 4	245 ± 5
c (km)		189 ± 19	167 ± 8	176 ± 3	170 ± 8
a/b	1.24	1.17 ± 0.17	1.25 ± 0.03	1.18 ± 0.02	1.18 ± 0.03
b/c	1.27	1.21 ± 0.17	1.40 ± 0.07	1.31 ± 0.03	1.44 ± 0.07
m (10^{18} kg)		27.2 ± 7.5	22.3 ± 3.6	24.3 ± 3.5	24.1 ± 3.2
ρ (g cm^{-3})		4.5 ± 1.4	3.7 ± 0.6	4.16 ± 0.64	3.99 ± 0.26

Notes. We list the volume-equivalent diameter D, dimensions along the major axes (a, b, c), sidereal rotation period P, pole ecliptic longitude λ and latitude β, mass m, and bulk density ρ. The uncertainties are reported at 1σ. K02: Kaasalainen et al. (2002) with diameter estimated from stellar occultation profiles by D11: Durech et al. (2011), S17: Shepard et al. (2017), H17: Hanus et al. (2017), D18: Drummond et al. (2018).

arbitrarily, ±30% as a reasonable interval for permitted variegation. The albedo distribution on the model is based mainly on lightcurves and is therefore not unique. However, both LSL (Kaasalainen et al. 2001) and Hapke (Hapke 1984) scattering laws resulted in almost identical albedo distributions.

We present in Fig. 1 the five SPHERE epochs, together with the corresponding projections of our shape model and of the radar-derived shape model. Our spin solution and volume-equivalent diameter D (226 ± 5 km) agree well with those reported in Shepard et al. (2017) and in several other studies (Table 1). The mass-deficit region (Shepard et al. 2017) is clearly visible in each SPHERE image, but its shape and size differ from the radar estimates. Furthermore, the projected area of Psyche on the plane of the sky is systematically underestimated by the radar model, as suggested by the differences in diameter along the three axes reported in Table 1. The polar region appears to be more flattened than suggested by the radar model. The albedo distribution (Fig. A.4) however closely matches the one presented by Shepard et al. (2017). The 3D shape model is depicted in Fig. A.3. One should keep in mind that only features visible and consistent in at least two images can be considered as genuine. If a feature is only seen in one image its plausibility depends on how reliable one assumes the post-processing of the image to be.

We then gathered 27 mass estimates and 15 diameter estimates of Psyche from the literature (Tables A.3 and A.4), which show significant scatter (Figs. A.5 and A.6). We therefore evaluated the reliability of each value and estimated a representative value of $(24.1 \pm 3.2) \times 10^{18}$ kg following the procedure developed by Carry et al. (2012) or Vernazza et al. (2018). We used this value together with our new size estimate to compute Psyche's bulk density of 3.99 ± 0.26 g cm^{-3}.

5. Surface topography

Although our observations covered only the northern hemisphere, they reveal the presence of two peculiar units with low and high brightness (Fig. 1). We named these two units after the twin witches related to the Metamorphoses, the latin novel of Apuleius in which Psyche is a character.

Of the two units, the dark unit *Meroe* clearly appears as a crater. Using the same approach as the one described in Vernazza et al. (2018), we measured its diameter to be in the 80−100 km range. We subsequently estimated the width and depth of the depression present in the contour of the *Panthia* unit to be ~90 km and ~10 km, respectively. Finally, the brightness profiles suggest that the *Panthia* unit is about 7% brighter than the surrounding areas, whereas the *Meroe* unit is 8% fainter.

6. Meteorite analogue

Whereas the density of Psyche derived in the present work (3.99 ± 0.26 g cm^{-3}) is incompatible at the 3-sigma level with the one of iron meteorites (~7.8 g cm^{-3}), it appears fully consistent with that of stony-iron meteorites such as mesosiderites (~4.25 g cm^{-3}; Britt & Consolmagno 2003) or the Steinbach meteorite (~4.1 g cm^{-3}; Britt & Consolmagno 2003).

Both mesosiderites and the unique Steinbach meteorite consist of a mixture of metal and pyroxene (orthopyroxene in the case of mesosiderites), a similar composition to that inferred for the surface of Psyche. Indeed, Vernazza et al. (2009) originally did not exclude a possible link between Psyche and mesosiderites on the basis of similar visible and near-infrared spectral properties, and recent laboratory measurements and observations (Cloutis et al. 2017; Sanchez et al. 2017) reinforce this finding. Hence, there is merit to the initial hypothesis by Davis et al. (1999), based on numerical simulations, that Psyche could be a plausible candidate parent body for mesosiderites.

Acknowledgements. Some of the work presented here is based on observations collected 1) at the European Organization for Astronomical Research in the Southern Hemisphere under ESO programs 086.C-0785 (PI Carry) and 199.C-0074 (PI Vernazza); 2) by SuperWASP (DR1) (Butters et al. 2010) as provided by the WASP consortium, and the computing and storage facilities at the CERIT Scientific Cloud, reg. no. CZ.1.05/3.2.00/08.0144 which is operated by Masaryk University, Czech Republic; and 3) the *W. M. Keck* Observatory, which is operated as a scientific partnership among the California Institute of Technology, the University of California and the National Aeronautics and Space Administration. The Observatory was made possible by the generous financial support of the *W. M. Keck* Foundation. This research has made use of the *Keck* Observatory Archive (KOA), which is operated by the *W. M. Keck* Observatory and the NASA Exoplanet Science Institute (NExScI), under contract with the National Aeronautics and Space Administration. M. Viikinkoski and M. Kaasalainen were supported by the Academy of Finland Centre of Excellence in Inverse Problems. B. Carry, A. Drouard, J. Grice and P. Vernazza were supported by CNRS/INSU/PNP. J. Hanus and J. Durech were supported by the grant 18-09470S of the Czech Science Foundation. This work has been supported by Charles University Research program No. UNCE/SCI/023. F. Marchis was supported by the National Science Foundation under Grant No 1743015. The research leading to these results has received

funding from the European Union's Horizon 2020 Research and Innovation Programme, under Grant Agreement no 687378. The authors wish to recognize and acknowledge the very significant cultural role and reverence that the summit of Mauna Kea has always had within the indigenous Hawaiian community. We are most fortunate to have the opportunity to conduct observations from this mountain. Thanks to all the amateurs worldwide who regularly observe asteroid lightcurves and stellar occultations. Co-authors of this study are amateurs who observed Psyche, and provided crucial data. The authors acknowledge the use of the Virtual Observatory tools Miriade: http://vo.imcce.fr/webservices/miriade/ (Berthier et al. 2008), TOPCAT: http://www.star.bris.ac.uk/~mbt/topcat/, and STILTS: http://www.star.bris.ac.uk/~mbt/stilts/ (Taylor 2005). This research used the SSOIS: http://www.cadc-ccda.hia-iha.nrc-cnrc.gc.ca/en/ssois facility of the Canadian Astronomy Data Centre operated by the National Research Council of Canada with the support of the Canadian Space Agency (Gwyn et al. 2012).

References

Avdellidou, C., Delbo', M., & Fienga, A. 2018, MNRAS, 475, 3419
Baer, J., & Chesley, S. R. 2017, AJ, 154, 76
Baer, J., Milani, A., Chesley, S. R., & Matson, R. D. 2008, BAAS, 40, 493
Baer, J., Chesley, S. R., & Matson, R. D. 2011, AJ, 141, 143
Berthier, J., Hestroffer, D., Carry, B., et al. 2008, LPI Contrib., 1405, 8374
Beuzit, J.-L., Feldt, M., Dohlen, K., et al. 2008, Proc. SPIE, 7014, 701418
Britt, D. T., & Consolmagno, G. J. 2003, Meteorit. Planet. Sci., 38, 1161
Butters, O. W., West, R. G., Anderson, D. R., et al. 2010, A&A, 520, L10
Carry, B. 2012, Planet. Space Sci., 73, 98
Carry, B., Kaasalainen, M., Merline, W. J., et al. 2012, Planet. Space Sci., 66, 200
Carry, B., Vachier, F., Berthier, J., & Team L. 2018, A&A, submitted
Chang, Y. C., & Chang, C. S. 1963, Acta Astron. Sin., 11, 139
Cloutis, E. A., Applin, D. M., Kiddell, C., et al. 2017, Lunar Planet. Sci. Conf., 48, 1228
Davis, D. R., Farinella, P., & Marzari, F. 1999, Icarus, 137, 140
Dollfus, A., & Geake, J. A. 1977, Eng. Sci., 285, 397
Dollfus, A., Auriere, M., & Santer, R. 1979, AJ, 84, 1419
Dotto, E., Barucci, M. A., Fulchignoni, M., et al. 1992, A&AS, 95, 195
Drummond, J., & Christou, J. 2008, Icarus, 197, 480
Drummond, J. D., Merline, W. J., Carry, B., et al. 2018, Icarus, 305, 174
Dunham, D. W., Herald, D., Frappa, E., et al. 2017, Asteroid Occultations, NASA Planetary Data System, EAR-A-3-RDR-OCCULTATIONS-V15.0
Ďurech, J., Kaasalainen, M., Herald, D., et al. 2011, Icarus, 214, 652
Elkins-Tanton, L. T., Asphaug, E., Bell, J. F., et al. 2017, Lunar Planet. Sci. Conf., 48, 1718
Fienga, A., Laskar, J., Morley, T., et al. 2009, A&A, 507, 1675
Fienga, A., Laskar, J., Kuchynka, P., et al. 2011, Celest. Mech. Dyn. Astron., 111, 363
Fienga, A., Manche, H., Laskar, J., Gastineau, M., & Verma, A. 2013, ArXiv e-prints [arXiv:1301.1510]
Fienga, A., Manche, H., Laskar, J., Gastineau, M., & Verma, A. 2014, Sci. Notes
Folkner, W. M., Williams, J. G., & Boggs, D. H. 2009, IPN Prog. Rep., 42, 1
Fusco, T., Mugnier, L. M., Conan, J. M., et al. 2003, in Adaptive Optical System Technologies II, eds. P. L. Wizinowich, & D. Bonaccini, Proc. SPIE, 4839, 1065
Goffin, E. 2014, A&A, 565, A56
Grice, J., Snodgrass, C., Green, S. F., Parley, N. R., & Carry, B. 2017, Asteroids, Comets, and Meteors: ACM 2017
Gwyn, S. D. J., Hill, N., & Kavelaars, J. J. 2012, Publ. Astron. Soc. Pac., 124, 579
Hanuš, J., Marchis, F., & Ďurech, J. 2013, Icarus, 226, 1045
Hanuš, J., Viikinkoski, M., Marchis, F., et al. 2017, A&A, 601, A114
Hapke, B. 1984, Icarus, 59, 41
Hardersen, P. S., Gaffey, M. J., & Abell, P. A. 2005, Icarus, 175,141
Harris, A. W., Young, J. W., Bowell, E., & Tholen, D. J. 1999, Icarus, 142, 173
Ivantsov, A. 2008, Planet. Space Sci., 56, 1857
Kaasalainen, M., Torppa, J., & Muinonen, K. 2001, Icarus, 153, 37
Kaasalainen, M., Torppa, J., & Piironen, J. 2002, Icarus, 159, 369
Kochetova, O. M. 2004, Sol. Sys. Res., 38, 66
Kochetova, O. M., & Chernetenko, Y. A. 2014, Sol. Sys. Res., 48, 295
Konopliv, A. S., Asmar, S. W., Folkner, W. M., et al. 2011, Icarus, 211, 401
Krasinsky, G. A., Pitjeva, E. V., Vasiliev, M. V., & Yagudina, E. I. 2001, Communications of IAA of RAS
Kuchynka, P., & Folkner, W. M. 2013, Icarus, 222, 243
Kuzmanoski, M., & Kovačević, A. 2002, A&A, 395, L17
Landsman, Z. A., Emery, J. P., Campins, H., et al. 2018, Icarus, 304, 58
Lupishko, D. F., Kiselev, N. N., Chernova, G. P., & Belskaya, I. N. 1980, Pisma v Astron. Zh., 6, 184
Lupishko, D. F., Belskaia, I. N., Tupieva, F. A., & Chernova, G. P. 1982, Astron. Vestnik, 16, 101
Margot, J. L., Pravec, P., Taylor, P., Carry, B., & Jacobson, S. 2015, Asteroid Systems: Binaries, Triples, and Pairs (Univ. Arizona Press), 355
Masiero, J. R., Mainzer, A. K., Grav, T., et al. 2012, ApJ, 759, L8
Matter, A., Delbo, M., Carry, B., & Ligori, S. 2013, Icarus, 226, 419
Moffat, A. 1969, A&A, 3, 455
Morrison, D., & Zellner, B. 2007, NASA Planet. Data Sys.
Mugnier, L. M., Fusco, T., & Conan, J.-M. 2004, JOSA A, 21, 1841
Neely, A. W. 1992, Minor Planet Bull., 19, 28
Ockert-Bell, M. E., Clark, B. E., Shepard, M. K., et al. 2008, Icarus, 195, 206
Pfleiderer, J., Pfleiderer, M., & Hanslmeier, A. 1987, A&AS, 69, 117
Pitjeva, E. V. 2013, Sol. Sys. Res., 47, 386
Pitjeva, E. V. 2010, in IAU Symp., eds. S. A. Klioner, P. K. Seidelmann, & M. H. Soffel, 261, 170
Reddy, V., Le Corre, L., O'Brien, D. P., et al. 2012, Icarus, 221, 544
Ryan, E. L., & Woodward, C. E. 2010, AJ, 140, 933
Sanchez, J. A., Reddy, V., Shepard, M. K., et al. 2017, AJ, 153, 29
Scheeres, D. J., Britt, D., Carry, B., & Holsapple, K. A. 2015, Asteroid Inter. Morphol., 745
Shepard, M. K., Clark, B. E., Ockert-Bell, M., et al. 2010, Icarus, 208, 221
Shepard, M. K., Taylor, P. A., Nolan, M. C., et al. 2015, Icarus, 245, 38
Shepard, M. K., Richardson, J., Taylor, P. A., et al. 2017, Icarus, 281, 388
Somenzi, L., Fienga, A., Laskar, J., & Kuchynka, P. 2010, Planet. Space Sci., 58, 858
Sykes, M., Brown, T., & Raugh, A. 1998, NASA Planet. Data Sys.
Takir, D., Reddy, V., Sanchez, J. A., Shepard, M. K., & Emery, J. P. 2017, AJ, 153, 31
Taylor, R. C. 1977, AJ, 82, 441
Taylor, M. B. 2005, in Astronomical Data Analysis Software and Systems XIV, eds. P. Shopbell, M. Britton, & R. Ebert, ASP Conf. Ser., 347, 29
Tedesco, E. F., & Taylor, R. C. 1985, Icarus, 61, 241
Tedesco, E. F., Taylor, R. C., Drummond, J., et al. 1983, Icarus, 54, 30
Thalmann, C., Schmid, H. M., Boccaletti, A., et al. 2008, Proc. SPIE, 7014, 70143F
Usui, F., Kuroda, D., Müller, T. G., et al. 2011, PASJ, 63, 1117
van Houten-Groeneveld, I., & van Houten, C. J. 1958, ApJ, 127, 253
Vasiliev, M. V., & Yagudina, E. I. 1999, Communications of IAA of RAS
Vernazza, P., Brunetto, R., Binzel, R. P., et al. 2009, Icarus, 202, 477
Vernazza, P., Castillo-Rogez, J., Beck, P., et al. 2017, AJ, 153, 72
Vernazza, P., Jorda, L., Hanuš, J., et al. 2018, A&A, 618, A154
Viateau, B. 2000, A&A, 354, 725
Viikinkoski, M. 2016, PhD Thesis, Tampere University of Technology
Viikinkoski, M., & Kaasalainen, M. 2014, Inverse Prob. Imaging, 8, 885
Viikinkoski, M., Kaasalainen, M., & Ďurech, J. 2015, A&A, 576, A8
Viswanathan, V., Fienga, A., Gastineau, M., & Laskar, J. 2017, Notes Scientifiques et Techniques de l'Institut de Mécanique Céleste, 39, 108
Warner, B. D. 2016, Minor Planet Bull., 43, 137
Weidenschilling, S. J., Chapman, C. R., Davis, D. R., et al. 1987, Icarus, 70, 191
Weidenschilling, S. J., Chapman, C. R., Davis, D. R., Greenberg, R., & Levy, D. H. 1990, Icarus, 86, 402
Yang, B., Wahhaj, Z., Beauvalet, L., et al. 2016, ApJ, 820, L35
Zhou, X.-H., & Yang, X.-Y. 1981, Acta Astron. Sin., 22, 378
Zhou, X. H., Yang, X. Y., & Wu, Z. X. 1982, Acta Astron. Sin., 23, 349
Zielenbach, W. 2011, AJ, 142, 120

Appendix A: Additional figures and tables

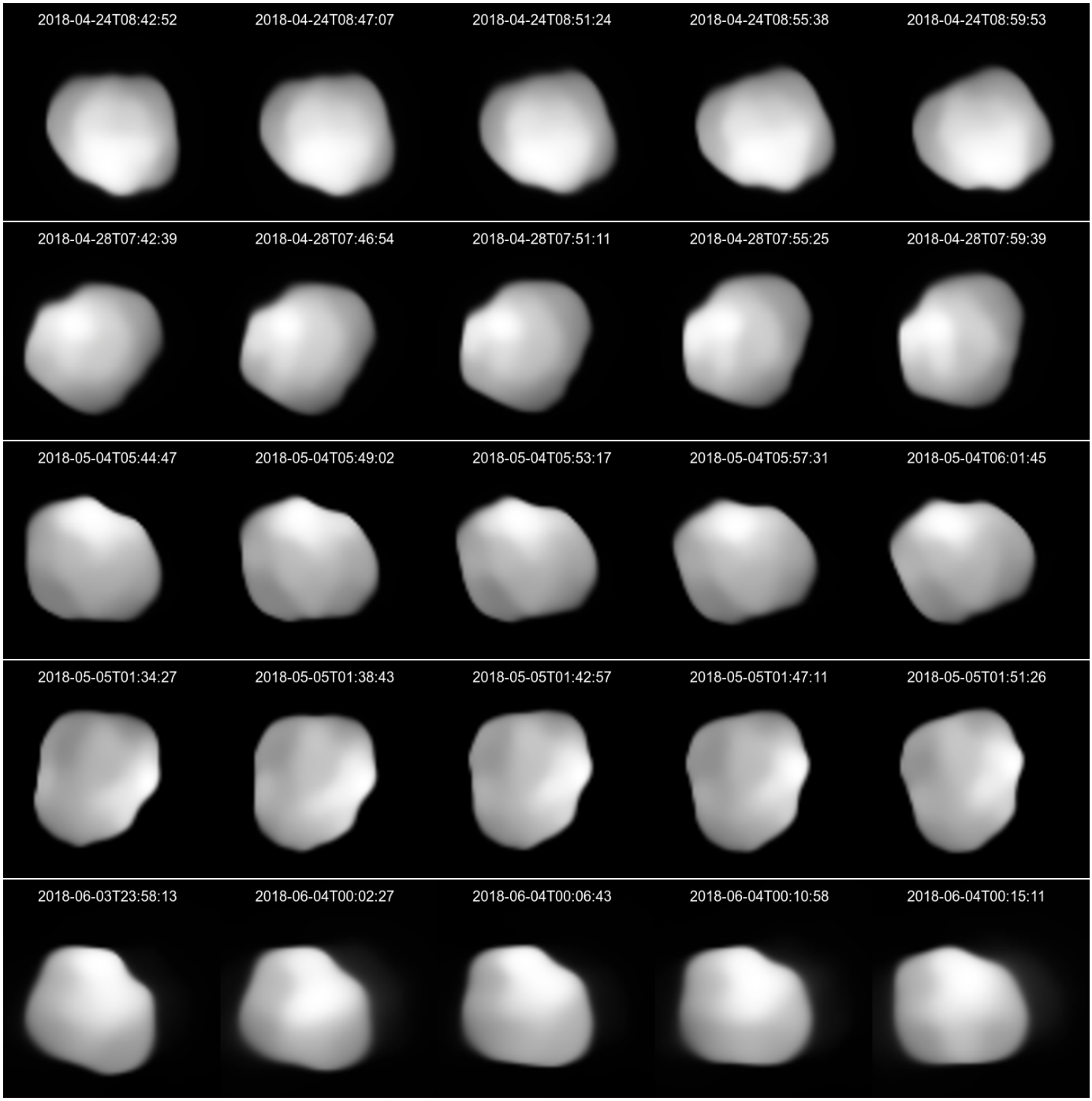

Fig. A.1. All 25 VLT/SPHERE/ZIMPOL images of Psyche obtained at five different epochs and deconvolved with the `Mistral` algorithm and a parametric PSF with a Moffat shape.

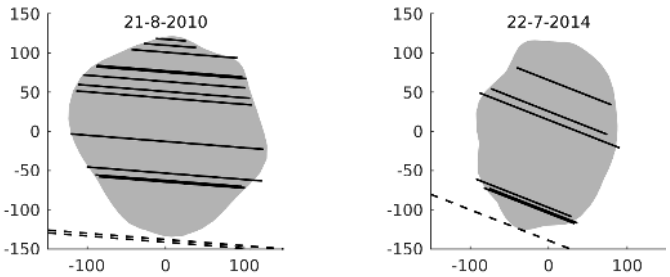

Fig. A.2. Observed occultation chords and the model silhouettes.

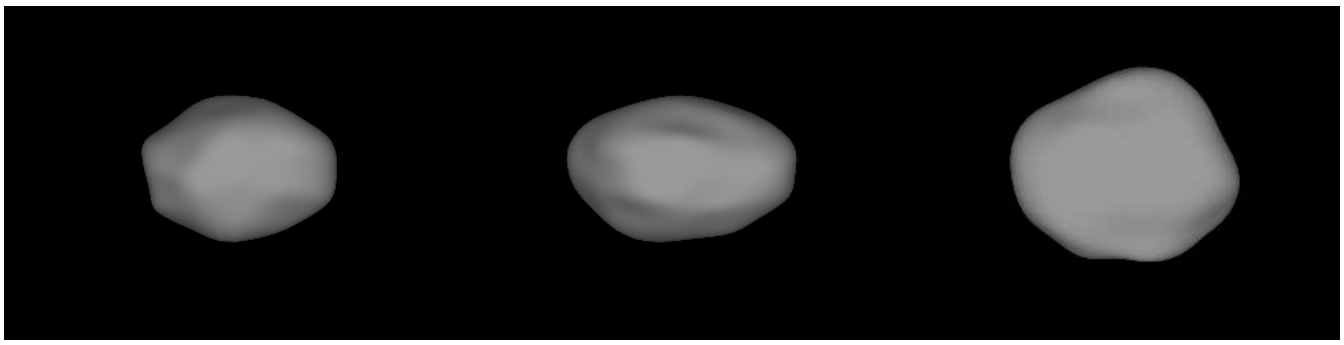

Fig. A.3. Shape model of Psyche. Viewing directions are from positive x, *y*, and z axes, respectively.

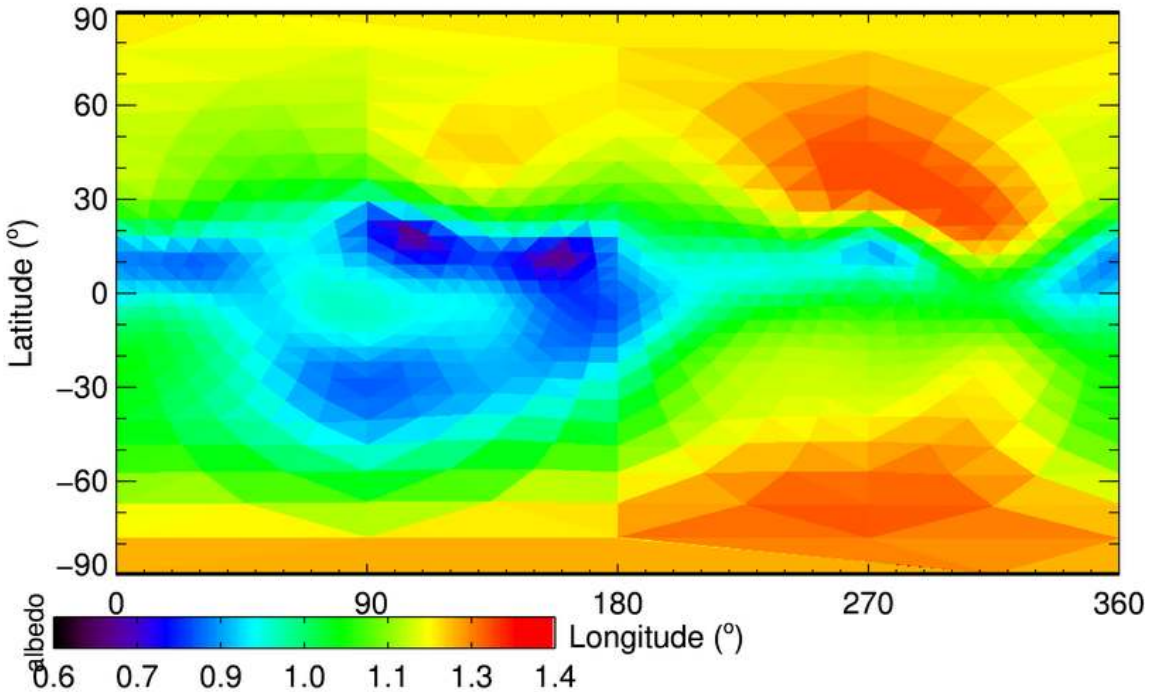

Fig. A.4. Albedo map distribution derived from the model showing the presence of a dark region near the equator (*Meroe*) and a bright feature near the poles at a longitude centered to 270 deg.

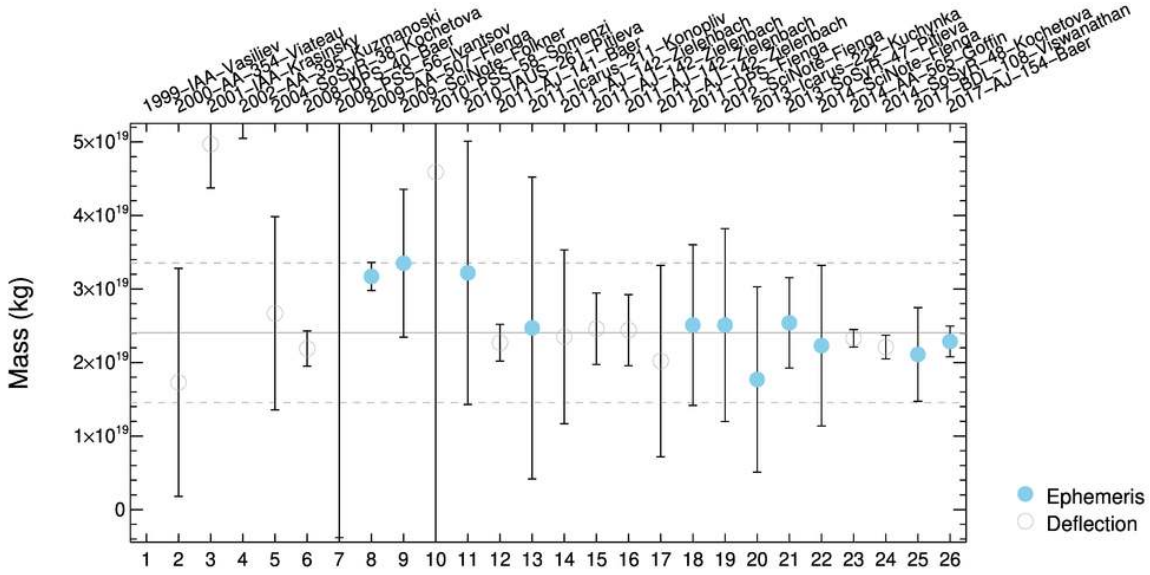

Fig. A.5. Available mass estimates for Psyche compiled from the literature. See Table A.3 for more details.

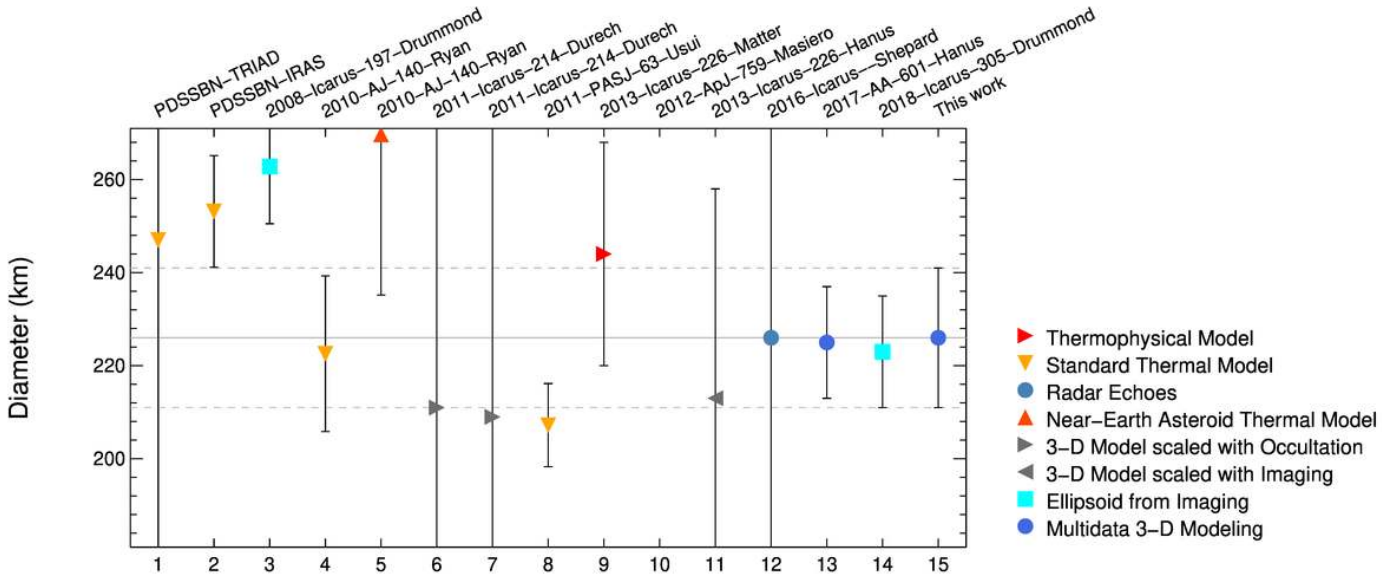

Fig. A.6. Available diameter estimates for Psyche compiled from the literature. See Table A.4 for more details.

Table A.3. Mass estimates ($\mathcal{M}$) of (16) Psyche collected in the literature.

#	Mass ($\mathcal{M}$) (kg)	ρ (g cc−1)	$\delta\rho$	Method	Sel.	Reference
1	$(2.53 \pm 1.07) \times 10^{20}$	41.860	6.542	DEFL	✗	Vasiliev & Yagudina (1999)
2	$(17.30 \pm 15.51) \times 10^{18}$	2.862	0.876	DEFL	✓	Viateau (2000)
3	$(4.97 \pm 0.60) \times 10^{19}$	8.223	0.637	DEFL	✗	Krasinsky et al. (2001)
4	$(6.72 \pm 1.67) \times 10^{19}$	11.118	1.181	DEFL	✗	Kuzmanoski & Kovacevic (2002)
5	$(2.67 \pm 1.31) \times 10^{19}$	4.418	0.782	DEFL	✓	Kochetova (2004)
6	$(2.19 \pm 0.24) \times 10^{19}$	3.623	0.274	DEFL	✓	Baer et al. (2008)
7	$(79.60 \pm 83.40) \times 10^{18}$	13.170	4.682	DEFL	✗	Ivantsov (2008)
8	$(3.17 \pm 0.19) \times 10^{19}$	5.245	0.364	EPHEM	✓	Fienga et al. (2009)
9	$(3.35 \pm 1.01) \times 10^{19}$	5.543	0.665	EPHEM	✓	Folkner et al. (2009)
10	$(4.59 \pm 5.79) \times 10^{19}$	7.594	3.233	DEFL	✓	Somenzi et al. (2010)
11	$(3.22 \pm 1.79) \times 10^{19}$	5.328	1.049	EPHEM	✓	Pitjeva (2010)
12	$(2.27 \pm 0.25) \times 10^{19}$	3.756	0.285	DEFL	✓	Baer et al. (2011)
13	$(24.70 \pm 20.52) \times 10^{18}$	4.087	1.164	EPHEM	✓	Konopliv et al. (2011)
14	$(2.35 \pm 1.18) \times 10^{19}$	3.888	0.701	DEFL	✓	Zielenbach (2011)
15	$(2.46 \pm 0.49) \times 10^{19}$	4.070	0.381	DEFL	✓	Zielenbach (2011)
16	$(2.44 \pm 0.48) \times 10^{19}$	4.037	0.378	DEFL	✓	Zielenbach (2011)
17	$(20.20 \pm 13.02) \times 10^{18}$	3.342	0.752	DEFL	✓	Zielenbach (2011)
18	$(2.51 \pm 1.09) \times 10^{19}$	4.153	0.662	EPHEM	✓	Fienga et al. (2011)
19	$(2.51 \pm 1.31) \times 10^{19}$	4.153	0.774	EPHEM	✓	Fienga et al. (2013)
20	$(17.70 \pm 12.60) \times 10^{18}$	2.929	0.722	EPHEM	✓	Kuchynka & Folkner (2013)
21	$(2.54 \pm 0.62) \times 10^{19}$	4.203	0.439	EPHEM	✓	Pitjeva (2013)
22	$(2.23 \pm 1.09) \times 10^{19}$	3.690	0.650	EPHEM	✓	Fienga et al. (2014)
23	$(2.33 \pm 0.12) \times 10^{19}$	3.855	0.264	DEFL	✓	Goffin (2014)
24	$(2.21 \pm 0.16) \times 10^{19}$	3.657	0.258	DEFL	✓	Kochetova & Chernetenko (2014)
25	$(2.11 \pm 0.64) \times 10^{19}$	3.491	0.420	EPHEM	✓	Viswanathan et al. (2017)
26	$(2.29 \pm 0.21) \times 10^{19}$	3.784	0.276	EPHEM	✓	Baer & Chesley (2017)
	$(2.40 \pm 0.95) \times 10^{19}$	Average				

Notes. For each, the 3σ uncertainty, computed density (using a diameter of 226.00 ± 5.00) and uncertainty, method, selection flag, and bibliographic reference are reported. The methods are DEFL: Deflection, EPHEM: Ephemeris.

Table A.4. Diameter estimates ($\mathcal{D}$) of (16) Psyche collected in the literature.

#	$\mathcal{D}$ (km)	$\delta\mathcal{D}$ (km)	ρ	$\delta\rho$	Method	Sel.	Reference
1	247.00	74.10	3.048	2.995	STM	✗	Morrison & Zellner (2007)
2	253.16	12.00	2.831	1.187	STM	✗	Sykes et al. (1998)
3	262.80	12.30	2.531	1.060	IM-TE	✗	Drummond & Christou (2008)
4	222.58	16.74	4.165	1.893	STM	✗	Ryan & Woodward (2010)
5	269.69	34.50	2.342	1.289	NEATM	✗	Ryan & Woodward (2010)
6	211.00	63.00	4.889	4.786	LCOCC	✗	Durech et al. (2011)
7	209.00	87.00	5.031	6.589	LCOCC	✗	Durech et al. (2011)
8	207.22	8.94	5.162	2.144	STM	✗	Usui et al. (2011)
9	244.00	24.00	3.162	1.558	TPM	✗	Matter et al. (2013)
10	288.29	13.89	1.917	0.806	NEATM	✗	Masiero et al. (2012)
11	213.00	45.00	4.753	3.548	LCIMG	✗	Hanus et al. (2013)
12	226.00	69.00	3.979	3.968	RADAR	✗	Shepard et al. (2017)
13	225.00	12.00	4.032	1.717	ADAM	✗	Hanus et al. (2017)
14	223.00	12.00	4.142	1.766	IM-TE	✗	Drummond et al. (2018)
15	226.00	15.00	3.979	1.759	ADAM	✓	This work
	226.00	15.00	Average				

Notes. For each, the 3σ uncertainty, method, selection flag, and bibliographic reference are reported. The methods are ADAM: Multidata 3D Modeling, IM-TE: Ellipsoid from Imaging, LCIMG: 3D Model scaled with Imaging, LCOCC: 3D Model scaled with Occultation, NEATM: Near-Earth Asteroid Thermal Model, RADAR: Radar Echoes, STM: Standard Thermal Model, TPM: Thermophysical Model.

Table A.5. Stellar occultations by Psyche.

Observer
(16) Psyche 2010-08-21
J. Brooks, Winchester, VA
S. Conard, Gamber, MD
D. Dunham, Seymour, TX
A. Scheck, Scaggsville, MD
D. Dunham, Seymour, TX
D. Dunham, Throckmorton, TX
C. Ellington, Highland Village, TX
P. Maley, Annetta South, TX
R. Tatum, Richmond, VA
P. Maley, Godley, TX
H.K. Abramson, Mechanicsville, VA
D. Caton, Boone, NC
E. Iverson, Athens, TX
R. Suggs, B. Cooke, Huntsville, AL
J. Faircloth, Kinston, NC
(16) Psyche 2014-07-22
G. Vaudescal, J. Caquel, R. Yken, J-P. Dupre
Jorge Juan, ES
Carles Schnabel, ES
C. Perello, A. Selva, ES
Peter Lindner, DE
Jan Manek, CZ
Peter Delincak, SK
Michal Rottenborn, CZ

Notes. We list the individual observers.